# Epitaxial lift-off of InGaAs solar cells from InP substrate using a strained AlAs/InAlAs superlattice as a novel sacrificial layer

F. Chancerel, P. Regreny, J.L. Leclercq, S. Brottet, M. Volatier, A. Jaouad, M. Darnon, S. Fafard, Nicholas Blanchard, Michel Gendry, et al.

Version of Record: https://www.sciencedirect.com/science/article/pii/S0927024819300790
Manuscript_5aaa5b89e65b8d2ffa5fc3020490eaa4

# Epitaxial lift-off of InGaAs solar cells from InP substrate using a strained AlAs/InAlAs superlattice as a novel sacrificial layer

F. Chancerel[⋆,1a, 2], P. Regreny[1a], J. L. Leclercq[1a], S. Brottet[1b], M. Volatier[2], A. Jaouad[2], M. Darnon[2], S. Fafard[2], N.P. Blanchard[3], M. Gendry[1a] and V. Aimez[2]

[1]Institut des Nanotechnologies de Lyon (INL)-UMR CNRS 5270- Université de Lyon,
[a]Ecole Centrale de Lyon, 36 avenue Guy de Collongue, 69134 Écully, France
[b]Institut National des Sciences Appliquées de Lyon, 7 avenue Jean Capelle 69621 Villeurbanne, France
[2]Laboratoire Nanotechnologies et Nanosystèmes, LN2-UMI CNRS 3463- Université de Sherbrooke,
3IT (Institut Interdisciplinaire d'Innovations Technologiques), 3000 Boulevard de l'université, Sherbrooke, QC, Canada
[3]Institut Lumière Matière (ILM)- UMR CNRS 5306- Université Claude Bernard Lyon 1, 69622, Villeurbanne, France
⋆francois.chancerel@usherbrooke.ca

## Abstract

In this work we present a new epitaxial lift-off (ELO) approach based on the use of a strained AlAs/InAlAs superlattice (SL) as sacrificial layer for InP related materials. Such an ELO process enables the fabrication and transfer of a thin active III-V heterostructure via its separation from its III-V parent substrate using selective chemical etching. The strategy is of particular interest for large area devices such as solar cells. The process studied here also allows the substrate reuse for a low-cost approach based on III-V-based device fabrication. In order to realize the ELO process on InP substrates, the main difficulty is the lack of lattice-matched materials offering the high chemical etching selectivity needed over both the substrate and the lattice-matched alloys of the active heterostructure. The present study therefore contributes effective strategies for overcoming the latter constraints. The AlAs/InAlAs SL was thus explored as a potential candidate as sacrificial layer for the InP lattice matched materials. The growth conditions of such SLs were investigated to produce low defect SLs compatible with the properties of an optimal sacrificial layer. The under-etching behavior of such SLs in a hydrofluoric acid-based solution was also studied in detail. The results show that advantageous under-etching rates, high enough for a full wafer detachment, combined with a low defect density, can be obtained with novel sacrificial layers based on such thin AlAs/InAlAs SL. Finally, the fabrication of solar cells via an active heterostructure grown over an optimized SL on a monolithic substrate and via a thin reported active heterostructure was performed. The solar cells perform well and demonstrate the suitability of such SLs as a sacrificial layer for InP related materials.

*Keywords: Superlattice; Epitaxial lift-off; Solar cell; III-V; Etching; Dislocations*

## Introduction

Low bandgap III-V alloys (eg. the ternary alloy InGaAs or quaternary alloys InGaAsP and InAlGaAs) lattice matched (LM) to Indium Phosphide (InP) substrates are of great interest in many applications, such as photodetectors, multi-junction solar cells (MJSC), quantum cascade lasers or other optoelectronic devices [1–5]. One of the major drawbacks for a wider development of theses alloy-based devices is the high cost of InP substrates especially for wide area devices like solar cells. The reuse of the InP substrate after each epitaxial growth should be a viable economic alternative. For this purpose epitaxial lift-off (ELO) seems to be the technological and financial solution to recycle substrates as mechano-chemical polishing steps (CMP) could be avoided [6,7].

The ELO process was first proposed in the 70's using AlAs as a release layer etched in a hydrofluoric acid (HF) solution in order to detach GaAs thin films from GaAs substrates [8,9]. This process has been widely studied and is well controlled on GaAs substrates using either $Al_xGa_{1-x}As$ (with $x>0.5$) or InAlP as a sacrificial layer (ScL) [10–13]. This technique has led to the realization of the most efficient single junction solar cell [14,15]. The choice of the ScL composition is critical in order to complete a full wafer process. Indeed high chemical selectivities (over both the substrate and the active heterostructure) and high under-etching rates (>1mm/h) are crucial parameters. It has also been shown, in various studies, that the thickness of the sacrificial layer plays an important role during the under-etching due to reactant/product diffusion related issues [16–18]. Regarding the results of these studies, it appears that the thickness of the ScL should be in the 5-10 nm range. Thicker layers lead to a slow down of the under-etching due to a higher amount of products to be evacuated from the etching front. On the contrary, too thin layer, typically less than 5 nm, leads to a sudden stop of the etching due to product deposition on the sidewalls of the active heterostructure-substrate based channel, especially for the detachment of large area devices [18].

Among LM alloys on InP, none offers the high chemical etching selectivity over both the InP substrate and the InGa(Al)(P)As low bandgap materials. AlAs could offer this selectivity in HF-based solutions [19] but has a lattice mismatch (3.6%) with InP that is too high. As calculated by D.M. Hwang et al. [20], the theoretical critical thickness for relaxation of such a tensile strained layer by 90° partial dislocations would be around 2.8 nm. D.M. Hwang et al. showed on TEM images that relaxation defects such as stacking faults with 90° partial dislocations appear in 3-5 nm-thick AlAs layers grown at 600°C on InP. Greater thicknesses lead to the formation of 60° and 90° perfect dislocations that allow the full relaxation of the strained material.

ELO of LM alloys on InP with AlAs as ScL has already been realized but no material quality studies were made and only areas less than 1 cm² were detached [21]. Solar cells or photodiodes fabricated with a AlAs layer thicker than 5 nm [22,23] have shown an increase of the dark current which probably comes from crystal defects

due to the ScL relaxation (e.g. dislocations) during the epitaxial growth and their propagation through the active layers above.

In order to overcome the thickness limitation of AlAs layers, we propose to use a superlattice (SL) which would allow a thicker ScL while preserving a high-quality material. Furthermore, during the chemical etching a SL can be considered as a single layer presenting an effective average composition integrating all the constituting SL atoms. AlAs/$In_{0,52}Al_{0,48}As$ and AlAs/InAs strained SLs grown on InP have already shown their capability to maintain good material structural qualities despite the high lattice mismatch between AlAs and InP [24,25]. Oxidation or under-etching rates of AlAs based layers (ie AlGaAs or InAlAs layers) or of AlAs based SLs are strongly dependent on the Al composition of such layers or SLs [26–28]. For our objective, the aim is to keep a high overall Al composition in the SL in order to obtain a high under-etching rate. To achieve this goal, we choose to use an AlAs/$In_{0.52}Al_{0.48}As$ (named InAlAs in the following) strained SL as a ScL that can be selectively etched with a HF solution.

In this study, the theoretical critical thickness for plastic relaxation of various AlAs/InAlAs SLs was calculated in order to choose the range of the SL thickness/composition to explore. Then we have focused our development on the material quality and defect density. A simple InP/InGaAs active structure was grown on an AlAs/InAlAs SL and characterized using photoluminescence (PL) mapping and transmission electron microscopy (TEM). Then the HF-based under-etching characteristics of such ScLs were determined and an InGaAs solar cell grown on an optimized SL was realized to assess the impact of structural defects on the targeted device performance. Finally, a thin crystalline solar cell on a host superstrate was realized via the etching of this optimized SL.

## 1. Theoretical critical thickness

Various models have been developed to obtain the theoretical critical thickness of strained layers, the most commonly used being that of W. Matthews and A. Blakeslee (MB) [29]. Nevertheless D.M. Hwang showed that the formation of stacking faults with partial dislocations occurred for thinner tensile strained layers than those deduced from the MB model [20]. He proposed a model allowing the calculation of two critical thicknesses, the first one being for the formation of 90° partial dislocations, the second one being for the formation of 60° perfect dislocations. By adapting this model to SL based on InAlAs barrier layers with thickness equal to $t_a$ and AlAs strained layers with thickness equal to $t_b$, using D. Houghton's assumptions [30], the critical thickness of the SL, defined as $h_c=N.t_b$ with $N$ is the number of periods inside the SL, can be expressed as follow:

$$h_c = Nt_b = \frac{\frac{b(1-\nu cos^2\theta)}{4\pi f cos\lambda(1+\nu)}}{1-\left(\frac{1}{2fcos\lambda sin\phi}\right)\left(\frac{1-\nu}{1+\nu}\right)\left(\frac{\gamma}{bG}\right)} ln\left(\frac{\alpha N(t_a+t_b)}{2bsin\phi}\right) \quad (1)$$

for 90° partial dislocations

$$h_c = Nt_b = \frac{b(1-\nu cos^2\theta)}{4\pi f cos\lambda(1+\nu)} ln\left(\frac{\alpha N(t_a+t_b)}{2bsin\phi}\right) \quad (2)$$

for 60° perfect dislocations

where $b$ is the norm of the Burger vector, $\nu$ the Poisson coefficient of the strained material, $f$ the misfit strain, $\theta$ the angle between the Burger vector and the dislocation line, $\lambda$ the angle between the Burger vector and the strain relief direction, $\Phi$ the angle between the stacking fault plane and the interfacial plane, G the shear modulus of AlAs, $\gamma$ the stacking fault energy per unit area and $\alpha$ a material-dependent parameter representing the contribution of the core energy (fixed to 4 for most semiconductors).

Resolving these equations for a SL composed of AlAs strained layers and 1 nm-thick InAlAs barrier layers, we can obtain the critical thickness $h_c=N.t_{AlAs}$ of the AlAs layers composing the SL as a function of N for a relaxation by 90° partial dislocations and 60° perfect dislocations (Fig. 1a). However in our case we are interested in the full critical thickness of the SL, taking into account of $t_{InAlAs}$: $h_c(SL)= (N-1).t_{InAlAs}+N.t_{AlAs}$, plotted as a function of N (Fig. 1b). We also calculated the average Al compositions, [Al], corresponding to the critical thicknesses of the SLs (also in Fig. 1b), with $[Al] = [(N-1)*t_a*0.48 + N*t_b]/[(N-1)*t_a + N*t_b]$. Indeed, it has already been observed that the under-etching rate of a AlGaAs/AlAs SL is similar to those of a single AlGaAs layer having the same average Al composition [31].

The region between the critical thickness curves for 90° partial dislocations and 60° perfect dislocations can be seen as a region were the layers are partially relaxed through a low density of staking faults with 90° partial dislocations. We can observe that using SLs will increase the critical thickness but also decrease the average Al

composition of the SL. A good compromise could be to use 3 AlAs layers as this allows the targeted 5 nm-limit thickness to be achieved and to keep a quite high average Al composition of more than 70%. Following these theoretical results, the experiments were realized with SLs composed of 2 to 4 AlAs layers and 1 nm-thick InAlAs barrier layers. A sample with a single 4.8 nm-thick AlAs layer was also realized as a reference.

## 2. Experimental

In order to determine the suitable design and the growth conditions of the aimed SL, experiments were carried out on heterostructures grown by solid-source molecular beam epitaxy (ssMBE) on semi-insulating InP(001) substrates. After InP substrate deoxidation at 500°C under a phosphorus ($P_2$) atmosphere, a 150 nm-thick InP buffer layer was grown at 470°C followed by the growth of the heterostructure itself with 1- the growth at $T_G$(SL) of the AlAs/InAlAs SL sandwiched by two 40 nm-thick LM InAlAs layers and 2- the growth at 470°C of the LM InGaAs/InP quantum well (QW) as the active layer with a 20 nm-thick LM InGaAs layer inserted between two 50 nm-thick InP layers (A-structure in Fig. 2a). The main SL design used was based on 3 AlAs layers and 2 InAlAs layers for the optimization of the material quality. For the under-etching study, various structures were used based on 2 to 4 AlAs layers in order to explore the effects of the total thickness and of the average Al composition of the SL on the under-etching rate.

For the SL growth at $T_G$(SL), the temperature is decreased during the first 40 nm-thick InAlAs layer and is then increased at the beginning of the first 50 nm-thick InP layer. On some samples, the growth of a sub-monolayer (ML)-thick (0.4 or 0.6 ML) compressive strained InAs was performed between the AlAs and InAlAs layers. This procedure is noted as “InAs incorporation”.

The structures were characterized by PL mapping using a 650 nm excitation line of an AlGaAs laser diode and an InGaAs photodetector. The defect characterization was realized by mapping the PL intensity at the emission peak maximum of the LM InGaAs/InP QW on a 1x1 mm² surface area with a 0.5 µm scan step. Cross sectional high-resolution transmission electron microscopy (HRTEM) was conducted on a JEOL 2100HT with an acceleration voltage of 200 kV in order to understand the defect formation and propagation into the structures. Lamellas perpendicular to the [1-10] crystal direction were prepared using the focused ion beam technique. The InGaAs solar cell structure (B-structure) was grown on a p++ doped ($1.10^{18}$ $cm^{-3}$) InP(001) substrate (Fig. 2b). The inverted structure (C-structure) used for the complete ELO process was realized on a semi-insulating InP (001) substrate (Fig. 2c). Doping was achieved using Si and Be as n- and p-type dopants, respectively.

## 3. Results and discussion

### 3.1. Study of AlAs/InAlAs SLs as a sacrificial layer

#### 3.1.1. Defect type and density in AlAs/InAlAs SLs

PL mappings realized on the LM InGaAs QW of different A-structures highlighted two main types of defects as illustrated in Figure 3. The first one is visible as black spots on the PL mappings. It can be noticed that these defects are aligned along the [1-10] direction. These defects are present over all the different structures (single AlAs layer and AlAs/InAlAs SLs). A second type of defect is visible as black lines along [1-10] and is present only in structures with (highly) strained SL grown at $T_G$(SL)=470 °C. Such PL signatures are characteristic of relaxation defects in tensile strained layers as already observed in relaxed InGaAs tensile strained layers grown on InP [32]. It can be clearly seen on Figure 3a that the 4.8 nm-thick AlAs layer grown at 400 °C is highly relaxed leading to a high defect density in the InGaAs QW grown on it. Therefore, such a layer could not be used as a sacrificial layer on InP. The PL mapping realized on a reference sample grown without any strained layer shows almost no defects confirming that the black zones observed on the PL mappings can be related to relaxation induced defects in the strained layer (or SL) propagating within the top structure.

In order to quantify the crystal quality of the various structures, the defect density was measured on PL maps counting both types of defect. As expected, the defect density is strongly increasing when the AlAs layers are thicker in the SLs composed of three AlAs layers and two 1 nm-thick InAlAs barrier layers (Fig. 4a). The corresponding PL mapping clearly shows this behavior, as on thicker SLs we observed almost continuous defect lines aligned along [1-10], while on thinner SLs we observed individual isolated defects. The sample grown with the thinner SL composed of 3x1.2 nm/2x1 nm AlAs/InAlAs shows a very low defect density close to that of the reference sample grown without SL ($4.9.10^3 cm^{-2}$ and $2.1.10^3 cm^{-2}$, respectively). However, the thickness and the global Al composition corresponding to this thin SL could be too low for fast under-etching. So, optimization of the growth parameters of a thicker SL composed of 3x1.5 nm/2x1 nm AlAs/InAlAs SL has been investigated

Therefore, the influence of the growth temperature $T_G$(SL) on the defect density of such a SL has been explored (Fig. 4b). The lower defect densities were obtained for $T_G$(SL) in the 400 °C-430 °C range. For upper

and lower $T_G$(SL) the defect density will greatly increase. On one hand, the defect density decrease with $T_G$(SL) is due to the lower thermal energy available for the formation of relaxation defects. On the other hand, a too low $T_G$(SL) can decrease the dislocation mobility therefore slowing down gathering [33]. Choosing the right temperature range allows decreasing by a factor 3 the defect density.

The last growth parameter investigated in this study was the growth of a sub-ML-thick InAs compressive strained layer on the AlAs layers which can partially compensate the AlAs tensile strain [34]. Even a partial strain compensation has already been demonstrated to be beneficial in order to diminish the relaxation of strained quantum wells [35]. As shown in Figure. 4c, the sub-ML InAs incorporation helps to decrease the defect density while having a really low impact on the overall Al composition. This last improvement leads to a global defect density of $5.3x10^3$ $cm^{-2}$ for the optimized SL which is close to $2.1x10^3$ $cm^{-2}$ measured for the reference sample (grown without SL). This low defect density can be obtained over a range of SL thickness $h_{SL}$ from 5 nm to 9 nm by changing the AlAs and InAlAs layer thicknesses, the average Al composition being nevertheless kept in the 80-85% range.

To better understand the origin of the observed defects a TEM study was conducted on three representative A-structures: 1- a single 4.8 nm-thick AlAs layer grown at $T_G$=400 °C (Fig. 5), 2- a 3x2.1 nm/2x1 nm AlAs/InAlAs SL grown at $T_G$(SL)=470°C (Fig. 6) and 3- a 3x2.1 nm/2x1 nm AlAs/InAlAs SL grown at $T_G$(SL)=400 °C (Fig. 7). In the single AlAs layer grown at 400 °C (with 0.6 ML InAs incorporation), we observe relaxation defects such as dislocations and stacking faults in the AlAs layer (Fig. 5ab). As shown on the fast Fourier transform (FFT) made around such defects (Fig. 5c), the stacking faults are bounded at both lower and upper interfaces by partial dislocations having antiparallel Burgers vectors. These defects are characteristic of the beginning of the relaxation of tensile strained layers as already observed by D.M. Hwang et al for AlAs layers grown on InP [36]. Concerning the dislocations, the FFT reveals that these dislocations can be either 60° or 90° perfect dislocations No surface corrugations are visible at the InAlAs/InP interface and on the InGaAs QW. For the 3x2.1 nm/2x1 nm AlAs/InAlAs SL grown at 470°C (with no InAs incorporation), we observe mainly microtwins nucleating in the tensile strained SL and, for some of them, crossing the upper part of the structure (Fig. 6ab). A few 60°perfect dislocations were also visible in the strained SL as revealed by the FFT shown in Figure 6c. Strong surface corrugations at the InAlAs/InP interface and on the InGaAs QW are also visible (Fig. 6a). For the 3x2.1 nm/2x1 nm AlAs/InAlAs SL grown at 400°C (with 0.6 ML InAs incorporation), no dislocations and stacking faults are observed in the strained SL and no significant surface corrugations are observed at the InAlAs/InP interface and on the InGaAs QW (Fig. 7a,b). This last result confirms the capacity of SLs with a thickness of AlAs layers up to 2.1 nm and grown at low $T_G$ to increase the critical thickness for plastic relaxation of tensile strained AlAs layers and therefore to limit the structural defect propagation through the structure.

### 3.1.2. Under-etching

The process to evaluate the under-etching rate starts with the deposition of a 200 nm-thick $SiO_2$ hard mask by plasma enhanced chemical vapor deposition on top of the structures. Following this deposition, photolithography was realized to define the mesa pattern (squares ranging from 100 x100 µm² to 600 x 600 µm²). The pattern was then transferred to the III-V structure using $CHF_3$ and $H_2/CH_4$ plasma reactive ion etching. Finally, the samples were dipped in a stirred HF solution. HF concentration, temperature and p-doping of the SL structure were varied to evaluate their effects on the under-etching selectivity.

The under-etching rate of the SL increases linearly with HF concentration (Fig. 8), this has already been observed with AlAs under-etching on GaAs [37]. We note that the thickness and the average Al composition seem to play an important role in the evolution of the under-etching rate.

In comparison we have observed that for bulk etching of LM InAlAs layers on InP – with 48% of Al content - the etching rate in a 40% vol. HF solution at 21°C is about 0.7 nm/min. We note a huge increase by a factor of $10^4$ to $10^5$ in the case of our thin InAlAs/AlAs SL, certainly due to the higher average Al composition.

In order to quantify the impact of the average Al composition, the thickness of various SLs was fixed to the value of 5 nm and the average Al composition was varied by changing either the number of AlAs layers and/or the ratio between the AlAs and InAlAs layer thicknesses. By averaging the Al composition in the SL, as shown in Figure 9a, the under-etching rate is increasing almost linearly when the average Al composition is increased. It is comparable with the trend obtained by P. Kumar et al. [26] on AlGaAs layers with Al compositions greater than 50%.

As these two results (linear variation with the HF concentration and the average Al composition) are both in accordance with the under-etching behavior of AlGaAs layers [26,37], the SL can be considered as an 'InAlAs'-like single layer during the selective wet under-etching with an average Al composition. This indicates that SLs are good candidates to enhance the under-etching rate while keeping a low defect density in the active layers.

In order to quantify the impact of the SL thickness on the under-etching rate an average Al composition of 85% was kept constant for various SL thicknesses (Fig. 9b). In the aim to keep a low defect density inside the upper layers, we need to use a thin sacrificial layer (lower than 10 nm for an average Al composition of 85%). It can be seen for such a range of thickness that the under-etching rate is increased linearly when the thickness of the SL is increased. This phenomenon can be related to diffusion limitation mechanisms [16,17].

Moreover, we have observed that the under-etching rate increases exponentially with the solution temperature (Fig. 10a). This trend has already been observed [18] and is well fitted with an Arrhenius equation:

$$V_e = V_{e,0} e^{-E_a/k_B T} \qquad (4)$$

With $V_e$ the under-etching rate; $V_{e,0}$ the under-etching rate at unlimited temperature; $E_a$ the activation energy; $T$the temperature and $k_B$ the Boltzmann constant.

From Table 1, we note that the value of activation energies and $V_{e0}$ of the two SLs on InP are close to those of 'thick' AlAs grown on GaAs. The quite low values obtained on SLs can be explained by both the lower average Al composition and the lower total thickness. Higher values were obtained with a 10 nm-thick AlAsP layer [18], but an external force was applied during the detachment of thin films. These obtained values of activation energies have confirmed that our SL under-etching process is diffusion rate limited. Nevertheless, the SL presented in Figure 10a has a low defect density (5 x $10^3$cm$^{-2}$ on PL mapping) and leads to an under-etching value larger than 1 mm/hr on our micrometric scale mesas but also on full 10 x10 mm² samples. For larger dimensions (e.g. full wafers), the under-etching rate of the SL should also be greatly enhanced by applying a radius of curvature on the detached thin film during ELO process at elevated temperature [18].

The effect of p-type doping concentration was also studied. For this, SLs composed of AlAs/InAlAs 3 x 1.2 nm/1 nm were doped at 3 different values from intrinsic to high concentrations. As shown in Figure 10b the doping is clearly impacting on the under-etching rate since the under-etching rate significantly increases by a factor of two for the SL doped at 1x$10^{19}$cm$^{-3}$ compared to the intrinsically doped SL (5x$10^{14}$ cm$^{-3}$). This effect can be related to a higher hole density at the etch-surface enhancing the chemical etching reaction [38].

### 3.2. InGaAs solar cell fabrication

In order to obtain a solar cell reference and assess the material quality grown over a 3 x 1.5 nm/2 x 1 nm AlAs/InAlAs SL (with 0.6 ML InAs incorporation) leading to a good compromise between the defect density, the Al composition and the ScL thickness, a solar cell test structure (B-structure in Fig. 2b) was grown on such a SL (named monolithic solar cell in the following). As shown in Figure 11a, the PL mapping of the solar cell structure indicates a low defect density (6.9.$10^3$/cm²) with no elongated defects. The defect density obtained is close to the one grown on a pristine p+ InP substrate, which indicates that the defects induced by such a SL are non-significant.

For the monolithic solar cell fabrication, a blanket Ti/Au (25/250 nm) contact metallization on the back surface and a front surface grid Ni/Ge/Au/Ni/Au (43/30/87/30/300 nm) contact were deposited by e-beam evaporation. Saw dicing was used to isolate individual 3.5 x 3.5 mm² cells. Finally, a selective $H_3PO_4$:$H_2O_2$:$H_2O$ wet etch was used to remove the top InGaAs contact layer between fingers of the grid contact.

An inverted solar cell structure (C-structure in Fig.2c) was grown over the same kind of SL in order to realize the ELO process. The first step was the deposition of Cr/Pt/Au layers (25/10/250 nm) used as a p contact, by e-beam evaporation on both the inverted structure and a 25 µm thick polyimide (kapton) foil. The structure was then bonded to the kapton foil using thermocompression bonding at 180 °C under 4 MPa for 45 min. The detachment of the thin film was then realized by immersion in a HF (40% vol. at 21 °C) solution. A 8 x 8 mm$^2$ membrane was detached in approximately 3 hours without any applied external force. This lead to an approximate under-etching rate of 1.3 mm/hr which is close to the 1.5 mm/hr measured on test structures. Just after the detachment the membrane is subject to a cleaning step composed of a residual particle etching in a $NH_4OH$ based solution and an etching of the InP and InAlAs protecting layers in HCl. Then, the thin crystal film follows the solar cell microfabrication procedure by applying a front surface grid Ni/Ge/Au/Ni/Au (43/30/87/30/300 nm) contact by e-beam evaporation followed by a selective $H_3PO_4$:$H_2O2$:$H_2O$ wet etch to remove the top InGaAs contact layer between fingers of the grid contact. Finally, 1 x 1 mm² solar cells were isolated by selective chemical etching.

The solar cells (based on B- and C-structures) were characterized by measuring one-sun current-voltage (J-V) at a temperature of 25°C with a home-made setup. The results presented in Table 2 are those of the best solar cells of each kind but the results were homogeneous on each sample and quite reproducible from one solar cell to another (variation of few mV for $V_{oc}$ and few 1/10 mA/cm² for $J_{sc}$).The characteristics of the InGaAs solar cell (B-structure) grown on the 3 x 1.5 nm/2 x1 nm AlAs/InAlAs SL (with 0.6 ML InAs incorporation) confirmed the

PL and TEM results as it demonstrated state of the art performance (Table 2). A high $V_{oc}$, is obtained indicating that this kind of SL will not affect the solar cell performance. The obtained $W_{oc}$ ($E_g/q$-$V_{oc}$) is 379 mV which is in the normal range for low band gap devices [39]. The thin crystalline film solar cell (C-structure) shows slightly lower performances with a 14 mV Voc drop which could be due to defects arising during the epitaxial layer lift-off and the different transfer processes or during the standard fabrication steps of the cell. The smaller size of the solar cells (1 x 1 mm2 versus 3.5 x 3.5 mm2) could also contribute to the decrease of Voc. Indeed, it has already been observed in the literature that decreasing the size of InGaAs solar cells could decrease Voc [40] in a similar manner to that of GaAs solar cells [41]. This decrease was related to arsenic oxide formation on the sides of the solar cell which has great chance to appear on the InGaAs solar cells presented here. The dark J-V curve measurements also shown an increase of the dark current density for the ELO cell compared to the monolithic one which is typical of lower size solar cells [41]. In any case this efficiency drop should be compensated by the optimization of the solar cell fabrication and of the handling of the thin crystalline films. Nevertheless, no slight shunting was visible after the detachment and sufficient $J_{sc}$ and FF were obtained confirming the suitability of such SLs as a sacrificial layer for low bandgap solar cell fabrication via the ELO process.

The performance of both solar cells should be slightly increased by applying an antireflection coating therefore increasing the short circuit current. The J-V characteristic (Fig. 12) shows a reasonably low fill factor (FF) which is common in the InGaAs based solar cells.

## 4. Conclusion

AlAs/InAlAs strained SLs have been studied as a sacrificial layer for the ELO process on InP substrates. The relaxation of the SLs leads mainly to stacking faults with partial dislocations and/or microtwins thus allowing a better management of the defect density compared to a single AlAs layer. The defect density can be thus strongly decreased for SLs with a thickness higher than 5 nm by optimizing the growth parameters (growth temperature and InAs sub-monolayer growth at the AlAs/InAlAs interface). However, high etching rates of such SLs in an HF based solution can be obtained only with highly defective SLs. Nevertheless, we have shown that it is possible to obtain a good compromise between a relatively high under-etching rate and a competitive optoelectronic device fabrication using a 3 x 1.5 to 2.1 nm/2 x 1 nm AlAs/InAlAs SL grown at $T_G$(SL)=400 °C (with 0.6 ML InAs incorporation). Our process allows a 30 µm/min etching rate (HF 40% vol. at 21°C) to be obtained with a non-significant increase of the induced defect density compared to a reference sample grown without any SL. This under-etching rate can be substantially increased by heating up the etching solution temperature or/and by a p-type doping of the SL. It is also expected that applying an external curvature to the detached thin films during the ELO process will enhance the under-etching rate.

Finally, thicker sacrificial layers can be obtained compared to a single AlAs layer which paved the way for an ELO process of large area low bandgap devices on InP substrates. Characteristic values of the under-etching rate are comparable to previously reported ones in the AlAs/GaAs system. InGaAs solar cells grown, as test devices, on this kind of sacrificial layer have shown state of the art results that confirm the potential of such superlattices. Lastly, the fabrication of solar cells via a thin crystal film detachment with a standard ELO procedure showed good performances demonstrating the suitability of such SLs as a sacrificial layer. The development of such a sacrificial layer paved the way for the fabrication of thin crystalline InGaAs film based solar cells via the full ELO process in order to obtain high efficiency multi-junction solar cells in a cost effective approach.

## 5. Acknowledgements

The authors would like to acknowledge the Auvergne Rhônes-Alpes region for its financial support. They would like also to thank Nanolyon and the CLYM platforms for facility access and technical support. LN2 is a joint International Research Laboratory (Unité Mixte Internationale UMI 3463) funded and co-operated in Canada by Université de Sherbrooke (UdeS) and in France by CNRS as well as Université de Lyon (UdL , especially including ECL, INSA Lyon, CPE) and Université Grenoble Alpes (UGA). It is also associated to the French national nanofabrication network RENATECH and is supported by the Fonds de Recherche du Québec Nature et Technologie (FRQNT).

## 6. References

[1] F. Dimroth, T.N.D. Tibbits, M. Niemeyer, F. Predan, P. Beutel, C. Karcher, E. Oliva, G. Siefer, D. Lackner, P. Fus-Kailuweit, A.W. Bett, R. Krause, C. Drazek, E. Guiot, J. Wasselin, A. Tauzin, T. Signamarcheix, Four-Junction Wafer-Bonded Concentrator Solar Cells, IEEE J. Photovoltaics. 6 (2016) 343–349. doi:10.1109/JPHOTOV.2015.2501729.

[2] J. Faist, F. Capasso, D.L. Sivco, C. Sirtori, A.L. Hutchinson, A.Y. Cho, Quantum Cascade Laser, Science (80-. ).

264 (1994) 553–556. doi:10.1126/science.264.5158.553.
[3] A. V. Thathachary, N. Agrawal, L. Liu, S. Datta, Electron Transport in Multigate InxGa1−xAs Nanowire FETs: From Diffusive to Ballistic Regimes at Room Temperature, Nano Lett. 14 (2014) 626–633. doi:10.1021/nl4038399.
[4] F. Valmorra, G. Scalari, K. Ohtani, M. Beck, J. Faist, InGaAs/AlInGaAs THz quantum cascade lasers operating up to 195 K in strong magnetic field, New J. Phys. 17 (2015) 23050. doi:10.1088/1367-2630/17/2/023050.
[5] J.C. Campbell, Recent advances in avalanche photodiodes, J. Light. Technol. 25 (2008) 109–121. doi:10.1109/LEOS.2008.4688747.
[6] J.S. Ward, T. Remo, K. Horowitz, M. Woodhouse, B. Sopori, K. VanSant, P. Basore, Techno-economic analysis of three different substrate removal and reuse strategies for III-V solar cells, Prog. Photovoltaics Res. Appl. 24 (2016) 1284–1292. doi:10.1002/pip.2776.
[7] K. Lee, J.D. Zimmerman, X. Xiao, K. Sun, S.R. Forrest, Reuse of GaAs substrates for epitaxial lift-off by employing protection layers, J. Appl. Phys. 111 (2012) 033527. doi:10.1063/1.3684555.
[8] M. Konagai, M. Sugimoto, K. Takahashi, High efficiency GaAs thin film solar cells by peeled film technology, J. Cryst. Growth. 45 (1978) 277–280. doi:10.1016/0022-0248(78)90449-9.
[9] E. Yablonovitch, T. Gmitter, J.P. Harbison, R. Bhat, Extreme selectivity in the lift-off of epitaxial GaAs films, Appl. Phys. Lett. 51 (1987) 2222–2224. doi:10.1063/1.98946.
[10] C.-W. Cheng, K.-T. Shiu, N. Li, S.-J. Han, L. Shi, D.K. Sadana, Epitaxial lift-off process for gallium arsenide substrate reuse and flexible electronics, Nat. Commun. 4 (2013) 1577. doi:10.1038/ncomms2583.
[11] G.J. Bauhuis, P. Mulder, E.J. Haverkamp, J.C.C.M. Huijben, J.J. Schermer, 26.1% thin-film GaAs solar cell using epitaxial lift-off, Sol. Energy Mater. Sol. Cells. 93 (2009) 1488–1491. doi:10.1016/j.solmat.2009.03.027.
[12] S. Moon, K. Kim, Y. Kim, J. Heo, J. Lee, Highly efficient single-junction GaAs thin-film solar cell on flexible substrate, Sci. Rep. 6 (2016) 30107. doi:10.1038/srep30107.
[13] S.R. Tatavarti, Z.S. Bittner, A. Wibowo, M.A. Slocum, G. Nelson, H. Kum, S.P. Ahrenkiel, S.M. Hubbard, Solar Energy Materials and Solar Cells Epitaxial Lift-off (ELO) of InGaP/GaAs/InGaAs solar cells with quantum dots in GaAs middle sub-cell, Sol. Energy Mater. Sol. Cells. 185 (2018) 153–157. doi:10.1016/j.solmat.2018.05.016.
[14] M.A. Green, K. Emery, Y. Hishikawa, W. Warta, E.D. Dunlop, Solar cell efficiency tables (Version 45), Prog. Photovoltaics Res. Appl. 23 (2015) 1–9. doi:10.1002/pip.2573.
[15] B.M. Kayes, H. Nie, R. Twist, S.G. Spruytte, F. Reinhardt, I.C. Kizilyalli, G.S. Higashi, 27.6% Conversion efficiency, a new record for single-junction solar cells under 1 sun illumination, in: 37th IEEE Photovolt. Spec. Conf., IEEE, 2011: pp. 4–8. doi:10.1109/PVSC.2011.6185831.
[16] K.S.R. Koteswara Rao, T. Katayama, S. Yokoyama, M. Hirose, Optimum Atomic Spacing for AlAs Etching in GaAs Epitaxial Lift-Off Technology, Jpn. J. Appl. Phys. 39 Part 2 (2000) L457–L459. doi:10.1143/JJAP.39.L457.
[17] J.J. Schermer, G.J. Bauhuis, P. Mulder, W.J. Meulemeesters, E. Haverkamp, M.M. a. J. Voncken, P.K. Larsen, High rate epitaxial lift-off of InGaP films from GaAs substrates, Appl. Phys. Lett. 76 (2000) 2131–2133. doi:10.1063/1.126276.
[18] a. T.J. van Niftrik, J.J. Schermer, G.J. Bauhuis, P. Mulder, P.K. Larsen, J.J. Kelly, A Diffusion and Reaction Related Model of the Epitaxial Lift-Off Process, J. Electrochem. Soc. 154 (2007) D629–D635. doi:10.1149/1.2779968.
[19] S. Sioncke, D.P. Brunco, M. Meuris, O. Uwamahoro, J. Van Steenbergen, E. Vrancken, M.M. Heyns, Etch Rates of Ge, GaAs and InGaAs in Acids, Bases and Peroxide Based Mixtures, ECS Trans. 16 (10) (2008) 451–460. doi:10.1149/1.2986802.
[20] D.M. Hwang, Strain relaxation in lattice-mismatched epitaxy, Mater. Chem. Phys. 40 (1995) 291–297. doi:10.1016/0254-0584(95)01485-3.
[21] D. Fan, K. Lee, S.R. Forrest, Flexible Thin-Film InGaAs Photodiode Focal Plane Array, ACS Photonics. 3 (2016) 670–676. doi:10.1021/acsphotonics.6b00042.
[22] H. Schumacher, T.J. Gmitter, H.P. LeBlanc, R. Bhat, E. Yablonovitch, M.A. Koza, High-speed InP/GaInAs photodiode on sapphire substrate, Electron. Lett. 25 (24) (1989) 1653–1654.
[23] K. Lee, K.-T. Shiu, J.D. Zimmerman, C.K. Renshaw, S.R. Forrest, Multiple growths of epitaxial lift-off solar cells from a single InP substrate, Appl. Phys. Lett. 97 (2010) 101107. doi:10.1063/1.3479906.
[24] N. Ohnoki, F. Koyama, K. Iga, Superlattice AlAs/AlInAs-oxide current aperture for long wavelength InP-based vertical-cavity surface-emitting laser structure, Appl. Phys. Lett. 73 (1998) 3262–3264. doi:10.1063/1.122738.
[25] E. Hall, A. Huntington, R.L. Naone, H. Kroemer, L.A. Coldren, Increased lateral oxidation rates of AlInAs on InP using short-period superlattices, J. Electron. Mater. 29 (2000) 1100–1104. doi:10.1007/s11664-004-0271-y.
[26] P. Kumar, S. Kanakaraju, D.L. Devoe, Sacrificial etching of AlxGa1-xAs for III-V MEMS surface micromachining, Appl. Phys. A. 88 (2007) 711–714. doi:10.1007/s00339-007-4032-7.
[27] J.M. Dallesasse, N.H. Jr, A.R. Sugg, T.A. Richard, N. El Zein, J.M. Dailesasse, N. Hoionyak, A.R. Sugg, T.A. Richard, Hydrolyzation oxidation of AlxGa1−xAsAlAsGaAs quantum well heterostructures and superlattices, Appl. Phys. Lett. 57 (1990) 38–41. doi:10.1063/1.103759.
[28] B. Koley, F.G. Johnson, O. King, S.S. Saini, M. Dagenais, A method of highly efficient hydrolyzation oxidation of III–V semiconductor lattice matched to indium phosphide, Appl. Phys. Lett. 75, 1264 (1999). doi:10.1063/1.124662.
[29] W. Matthews, A.E. Blakeslee, Defects in epitaxial multialyers, J. Cryst. Growth. 27 (1974) 118–125. doi:10.1016/S0022-0248(74)80055-2.
[30] D.C. Houghton, D.D. Perovic, J. Baribeau, G.C. Weatherly, Misfit strain relaxation in GexSi1-x/Si heterostructures: The structural stability of buried strained layers and strained-layer superlattices, J. Appl. Phys. 67 (1990) 1850. doi:10.1063/1.345613.
[31] H.Y. Lee, X. Letartre, J.L. Leclercq, P. Viktorovitch, L. Konczewicz, M. Sadowski, J.L. Robert, Gaalas-based

micromachined accelerometer, High Press. Res. 19 (2000) 347–351. doi:10.1080/08957950008202576.
[32] S.K. Krawczyk, M. Gendry, C. Klingelhöfer, T. Venet, M. Buchheit, R. Blanchet, G. Hollinger, Application of spectrally resolved scanning photoluminescence to assess relaxation processes of InGaAs and InAlAs layers strained in compression and tension, Mater. Sci. Eng. B. 42 (1996) 146–152. doi:10.1016/S0921-5107(96)01696-0.
[33] T. Ward, A.M. Sánchez, M. Tang, J. Wu, H. Liu, D.J. Dunstan, R. Beanland, Design rules for dislocation filters, J. Appl. Phys. 116 (2014) 063508. doi:10.1063/1.4892162.
[34] D.C. Houghton, M. Davies, M. Dion, Design criteria for structurally stable, highly strained multiple quantum well devices, Appl. Phys. Lett. 64 (1994) 505–507. doi:10.1063/1.111111.
[35] K. Bacher, S. Massie, M. Seaford, Molecular beam epitaxy of strain-compensated InGaAs/GaAsP quantum-well intersubband photodetectors, J. Cryst. Growth. 175–176 (1997) 977–982. doi:10.1016/S0022-0248(96)01007-X.
[36] D.M. Hwang, R. Bhat, S.A. Schwarz, Y. Chen, Partial Dislocations and Critical Thicknesses for Strained Layer Relaxation, in: Mat. Res. Soc. Symp. Proc. Vol. 263., 1992: pp. 421–426.
[37] M.M.A.J. Voncken, J.J. Schermer, G. Maduro, G.J. Bauhuis, P. Mulder, P.K. Larsen, Influence of radius of curvature on the lateral etch rate of the weight induced epitaxial lift-off process, Mater. Sci. Eng. B. 95 (2002) 242–248. doi:10.1016/S0921-5107(02)00240-4.
[38] M.M.A.J. Voncken, J.J. Schermer, a. T.J. van Niftrik, G.J. Bauhuis, P. Mulder, P.K. Larsen, T.P.J. Peters, B. de Bruin, A. Klaassen, J.J. Kelly, Etching AlAs with HF for Epitaxial Lift-Off Applications, J. Electrochem. Soc. 151 (2004) G347–G352. doi:10.1149/1.1690293.
[39] R.R. King, D.C. Law, K.M. Edmondson, C.M. Fetzer, G.S. Kinsey, H. Yoon, R.A. Sherif, N.H. Karam, 40% efficient metamorphic GaInP/GaInAs/Ge multijunction solar cells, Appl. Phys. Lett. 90 (2007) 183516. doi:10.1063/1.2734507.
[40] J.L. Cruz-Campa, A. Tauke-Pedretti, J.G. Cederberg, C.A. Sanchez, G.R. Girard, C. Alford, B.A. Aguirre, I. Luna, M. Okandan, J.S. Nelson, G.N. Nielson, Power maximization in III-V sub-millimeter, radial front contacted cells for thin micro-concentrators, in: 2014 IEEE 40th Photovolt. Spec. Conf., IEEE, Denver, CO, USA, 2014: pp. 471–475. doi:10.1109/PVSC.2014.6924961.
[41] P. Espinet-González, I. Rey-Stolle, M. Ochoa, C. Algora, I. García, E. Barrigón, Analysis of perimeter recombination in the subcells of GaInP/GaAs/Ge triple-junction solar cells, Prog. Photovoltaics Res. Appl. 23 (2015) 874–882. doi:10.1002/pip.2501.
[42] I. Mathews, D. O'Mahony, A. Gocalinska, E. Pelucchi, K. Thomas, A.P. Morrison, B. Corbett, InAlAs and InGaAs solar cell development for use in monolithic triple-junction solar cells with improved sprectrum splitting, in: 28th Eur. Photovolt. Sol. Energy Conf. Exhib., EUPVSEC, 2013: pp. 356–360. doi:110.4229/28thEUPVSEC2013-1AV.2.40.
[43] H.J. Schimper, Z. Kollonitsch, K. Möller, U. Seidel, U. Bloeck, K. Schwarzburg, F. Willig, T. Hannappel, Material studies regarding InP-based high-efficiency solar cells, J. Cryst. Growth. 287 (2006) 642–646. doi:10.1016/j.jcrysgro.2005.10.121.

# Figure captions

*Figure 1 : Theoretical critical thickness: a) $h_c=N.t_{AlAs}$ and b) $h_c(SL)=(N-1)t_{InAlAs}+N.t_{AlAs}$ in AlAs/InAlAs SLs and their corresponding average Al composition, as a function of the number N of AlAs strained layers inside SLs with 1 nm-thick InAlAs barrier layers.*

*Figure 2: a) A-structure: Structure used for the material characterizations and the under-etching rate measurements (x and y represent, respectively, AlAs and InAlAs thicknesses), b) B-structure: monolithic solar cell structure and c) C-structure: inverted solar cell structure, grown on a 3x1.5 nm/2x1 nm AlAs/InAlAs SL.*

*Figure 3: 1x1mm² PL intensity mapping of A-structures with the InGaAs QW grown on: a) a 4,8 nm-thick AlAs single layer ($T_G$(AlAs)=400°C; 0.6 ML InAs incorporation) b) a 3x2.1 nm/2x1 nm AlAs/InAlAs SL ($T_G$(SL)=470°C; no InAs incorporation), c) a 3x1.5 nm/2x1 nm AlAs/InAlAs SL ($T_G$(SL)=470°C; no InAs incorporation), d) a reference sample grown without SL.*

*Figure 4: Defect density measured on 1x1 mm² PL mappings as a function of: a) the total thickness hSL of SLs composed of three AlAs layers of various thickness and two 1 nm-thick InAlAs layers (TG(SL)=470°C; no InAs incorporation) b) the growth temperature TG(SL) of a 3x1.5 nm/2x1 nm AlAs/InAlAs SL (no InAs incorporation,) c) the amount of InAs incorporation for a 3x1.5 nm/2x1 nm SL (TG(SL)=400°C).*

*Figure 5: a) TEM image (dark-field g111) and b) HRTEM image ([1-10] zone axis) of the A-structure with a ScL composed of a single 4.8 nm-thick AlAs layer ($T_G$(SL)=400 °C; 0.6 ML InAs incorporation). The arrows in b) indicate the location of stacking faults (green) with partial dislocations (yellow), 90° perfect dislocations (red) and 60° perfect dislocations (blue), as revealed by the FFT realized on these defects and illustrated in c) with: a stacking fault (green) with the Burgers circuits (in yellow) indicating that the stacking fault is bounded at both lower and upper interfaces by partial dislocations having antiparallel Burgers vectors (in red), two 90° perfect dislocations with Burgers circuits in red (the Burger vector is in blue) and one 60° perfect dislocation with the Burgers circuit in blue (the Burgers vector is in red). The [001] growth direction is represented by a black arrow in a) and b).*

*Figure 6: a) Dark-field TEM image (g002) and b) HRTEM image ([1-10] zone axis) of the A-structure with a ScL composed of a 3x2.1 nm/2x1 nm AlAs/InAlAs SL ($T_G$(SL)=470°C; no InAs incorporation). The purple arrows in b) indicate microtwins and the blue arrow indicates the location of a 60° perfect dislocation as revealed by the FFT realized on this defect and illustrated in c) with the Burgers circuit in blue (the Burgers vector is in red). The [001] growth direction is represented by a black arrow in a) and b).*

*Figure 7: a) Dark-field TEM image (g002) and b) HRTEM image ([1-10] zone axis) of the A-structure with a ScL composed of a 3x2.1 nm/2x1 nm AlAs/InAlAs SL ($T_G$(SL)=400°C; 0.6 ML InAs incorporation), The [001] growth direction is represented by a black arrow.*

*Figure 8: Under-etching rate at 21°C as a function of the HF concentration for different ScL (SL) thicknesses and average Al compositions.*

*Figure 9: Under-etching rate at 21°C as a function of: a) the average Al composition of the ScL (SL) ($h_{SL}$ is kept at 5 nm) and b) the ScL (SL) thickness (the average Al composition is kept at 85%) in a 40% vol. HF solution.*

*Figure 10: Under-etching rate as a function of: a) the temperature of a 20% vol. HF solution for: a 3x2.1 nm/2x1 nm AlAs/InAlAs SL on InP ([Al]=86% and $h_{SL}$=8.3 nm blue circle), a 3x1.5 nm/2x1 nm AlAs/InAlAs SL on InP ([Al]=84% and $h_{SL}$=6.5 nm, red triangle), and a 30 nm-thick AlAs layer on GaAs. The red lines represent the best fits obtained using eq. (4) and b) the doping of a 3x1.2 nm/2x1 nm AlAs/InAlAs SL ([Al]=80.8% and $h_{SL}$=5.6 nm) in a 40% vol. HF solution at 21°C.*

*Figure 11: 1 x 1 $mm^2$ PL intensity mapping of the a) monolithic solar cell structure (B-structure) and b) inverted solar cell structure (C-structure) grown over a AlAs/InAlAs 3 x 1.5 nm/2 x 1 nm.*

*Figure 12: J-V under 1 sun AM1.5D illumination of the InGaAs solar cells grown on a 3x1.5 nm/2x1 nm AlAs/InAlAs SL ($T_G$(SL)=400°C; 0.6 ML InAs incorporation) via a monolithic approach (B-structure) and the ELO approach (C-structure).*

# Tables

| ScL type | $Ve_0$ (mm/hr) | Ea (eV) |
|---|---|---|
| 3 x 1.5 nm/2 x 1 nm / InP | $7.80x10^4$ | 0.23 |
| 3 x 2.1 nm/2 x 1 nm / InP | $2.75x10^5$ | 0.26 |
| AlAs 30 nm / GaAs | $2.21x10^5$ | 0.23 |

*Table 1: Under-etching rate at unlimited temperature and activation energy of various sacrificial layers (from Fig. 10a).*

| Source | Voc (mV) | Jsc ($mA/cm^2$) | FF (%) |
|---|---|---|---|
| This work monolithic | 353 ± 3 | 33.2 ± 0.5 | 69.9 ± 0.5 |
| This work ELO | 339 ± 3 | 33.8 ± 0.5 | 69.4 ± 0.5 |
| Matthews[42] | 357 ± 3 | 38.2 ± 0.5 | 69 ± 0.5 |
| Schimper[43] | 352 ± 3 | 47.3 ± 0.5 | - |

*Table 2: Performances of the InGaAs solar cells grown on a 3x1.5 nm/2x1 nm AlAs/InAlAs SL (TG(SL)=400°C; 0.6 ML InAs incorporation) via a monolithic approach (B-structure) and the ELO approach (C-structure) compared to other InGaAs solar cells.*

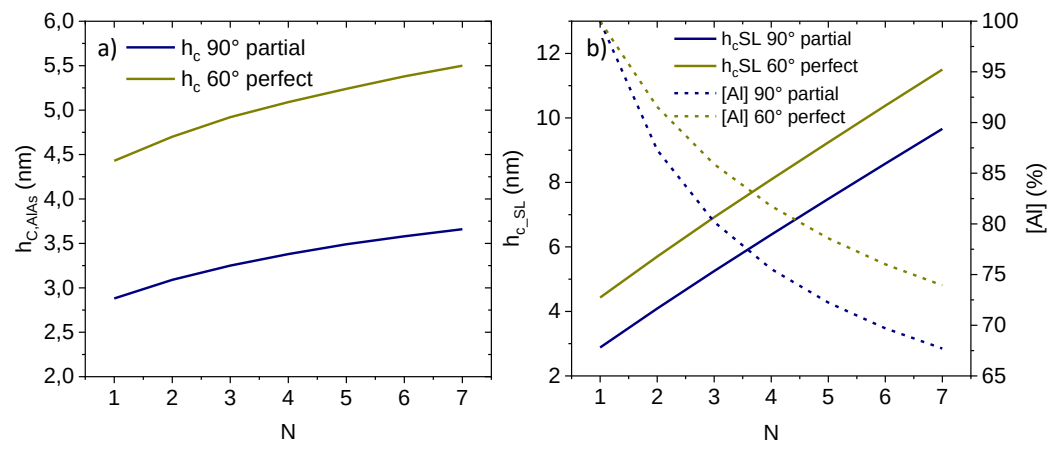
a)
h_c 90° partial
h_c 60° perfect
h_C,AlAs (nm)
N
b)
h_cSL 90° partial
h_cSL 60° perfect
[Al] 90° partial
[Al] 60° perfect
h_c_SL (nm)
[Al] (%)
N

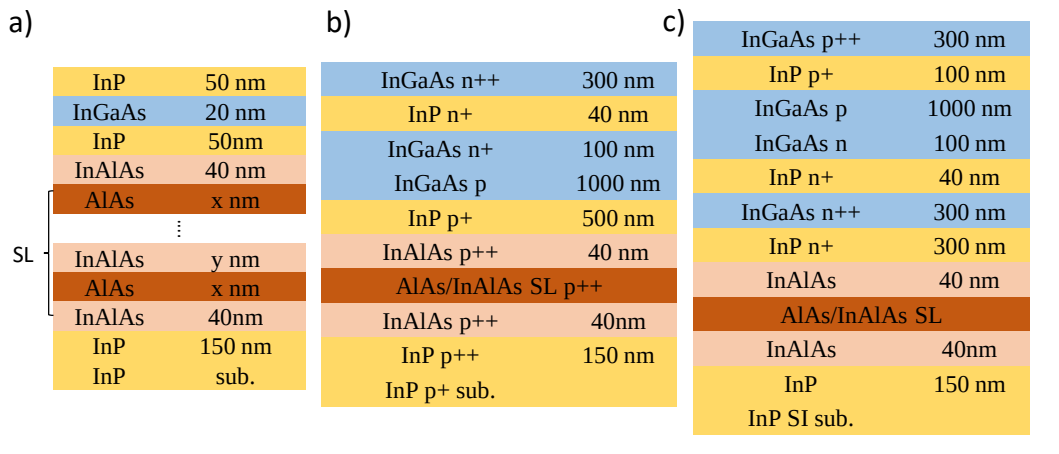
a)
InP 50 nm
InGaAs 20 nm
InP 50nm
InAlAs 40 nm
AlAs x nm
SL
InAlAs y nm
AlAs x nm
InAlAs 40nm
InP 150 nm
InP sub.
b)
InGaAs n++ 300 nm
InP n+ 40 nm
InGaAs n+ 100 nm
InGaAs p 1000 nm
InP p+ 500 nm
InAlAs p++ 40 nm
AlAs/InAlAs SL p++
InAlAs p++ 40nm
InP p++ 150 nm
InP p+ sub.
c)
InGaAs p++ 300 nm
InP p+ 100 nm
InGaAs p 1000 nm
InGaAs n 100 nm
InP n+ 40 nm
InGaAs n++ 300 nm
InP n+ 300 nm
InAlAs 40 nm
AlAs/InAlAs SL
InAlAs 40nm
InP 150 nm
InP SI sub.

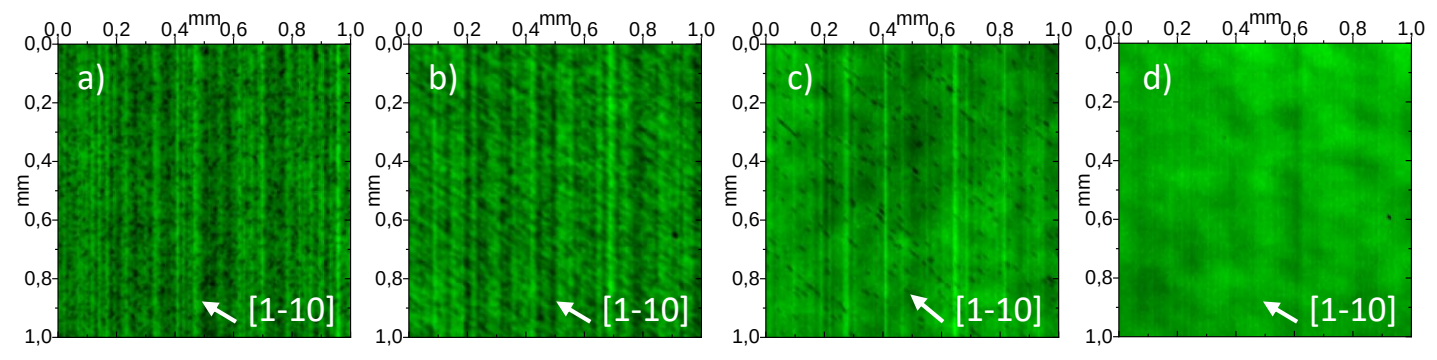
a)
b)
c)
d)
mm
0,0
0,2
0,4
0,6
0,8
1,0
[1-10]

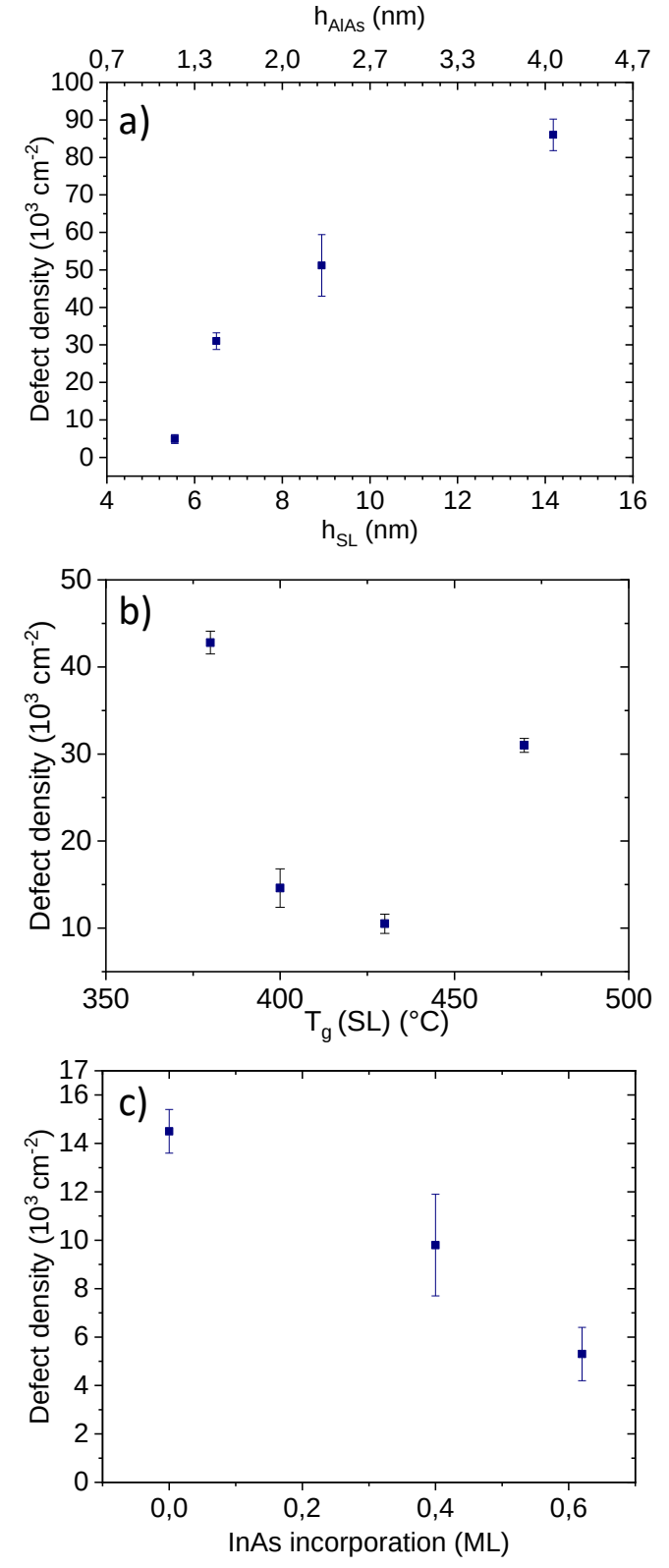
h_AlAs (nm)
0,7
1,3
2,0
2,7
3,3
4,0
4,7
a)
Defect density (10^3 cm^-2)
h_SL (nm)
b)
Defect density (10^3 cm^-2)
T_g (SL) (°C)
c)
Defect density (10^3 cm^-2)
InAs incorporation (ML)

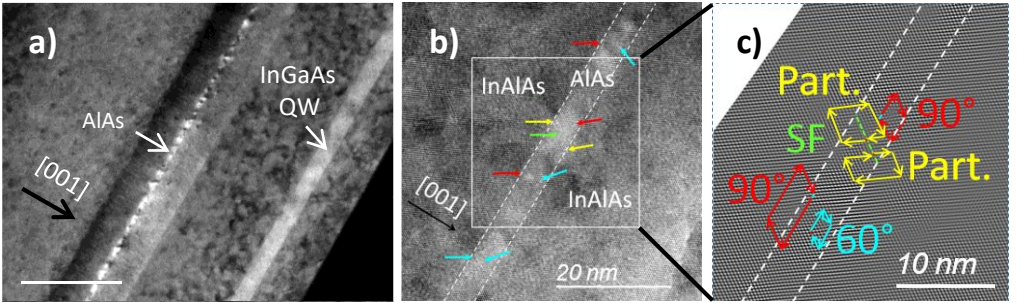
a)
InGaAs
QW
AlAs
[001]
b)
InAlAs
AlAs
InAlAs
[001]
20 nm
c)
Part.
SF
90°
Part.
90°
60°
10 nm

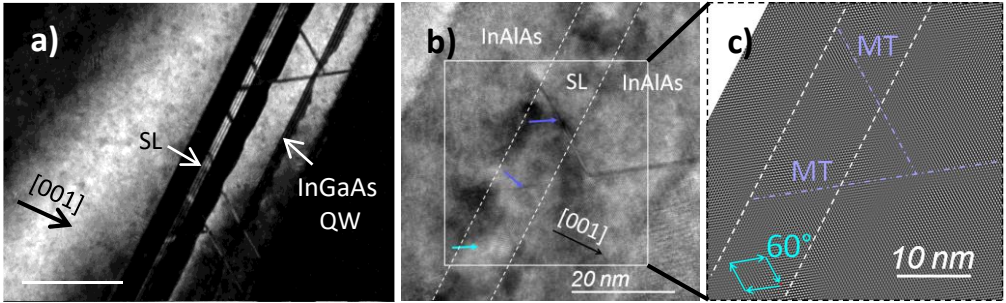
a)
SL
InGaAs
QW
[001]
b)
InAlAs
SL
InAlAs
[001]
20 nm
c)
MT
MT
60°
10 nm

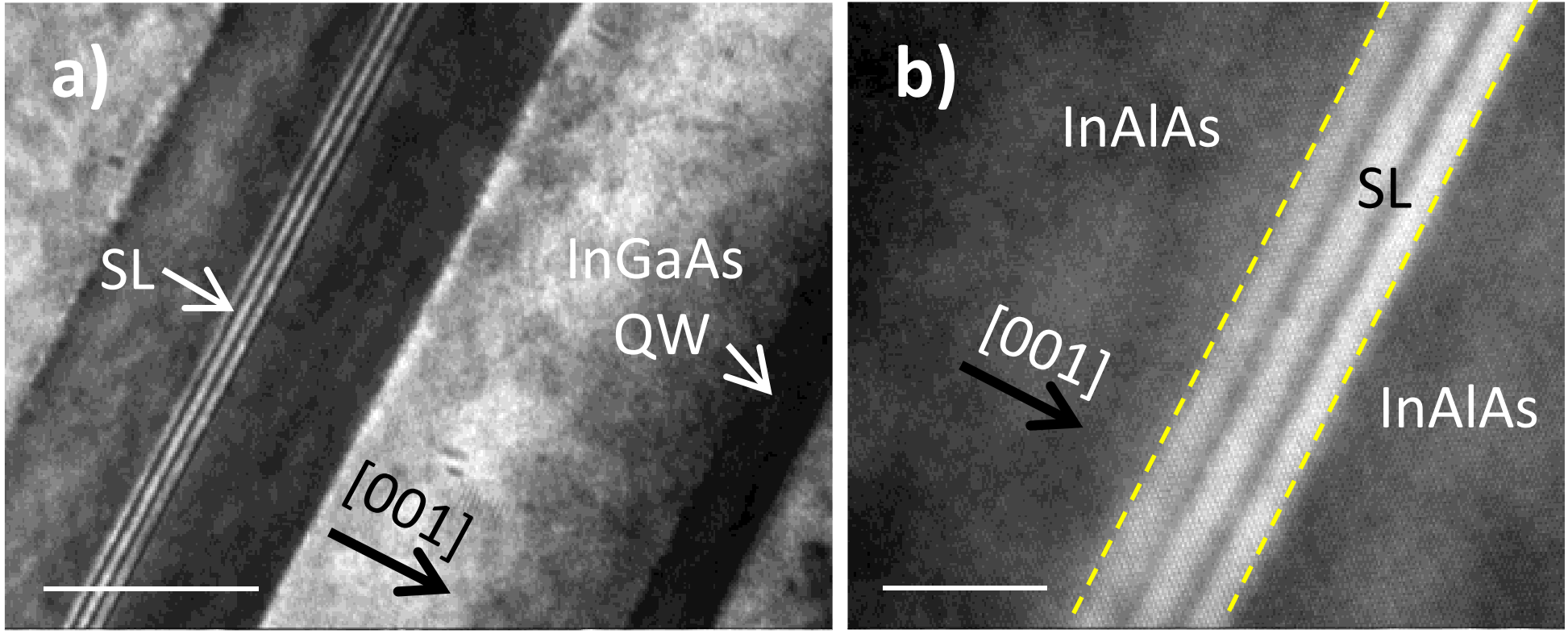
a)
SL
InGaAs
QW
[001]
b)
InAlAs
SL
[001]
InAlAs

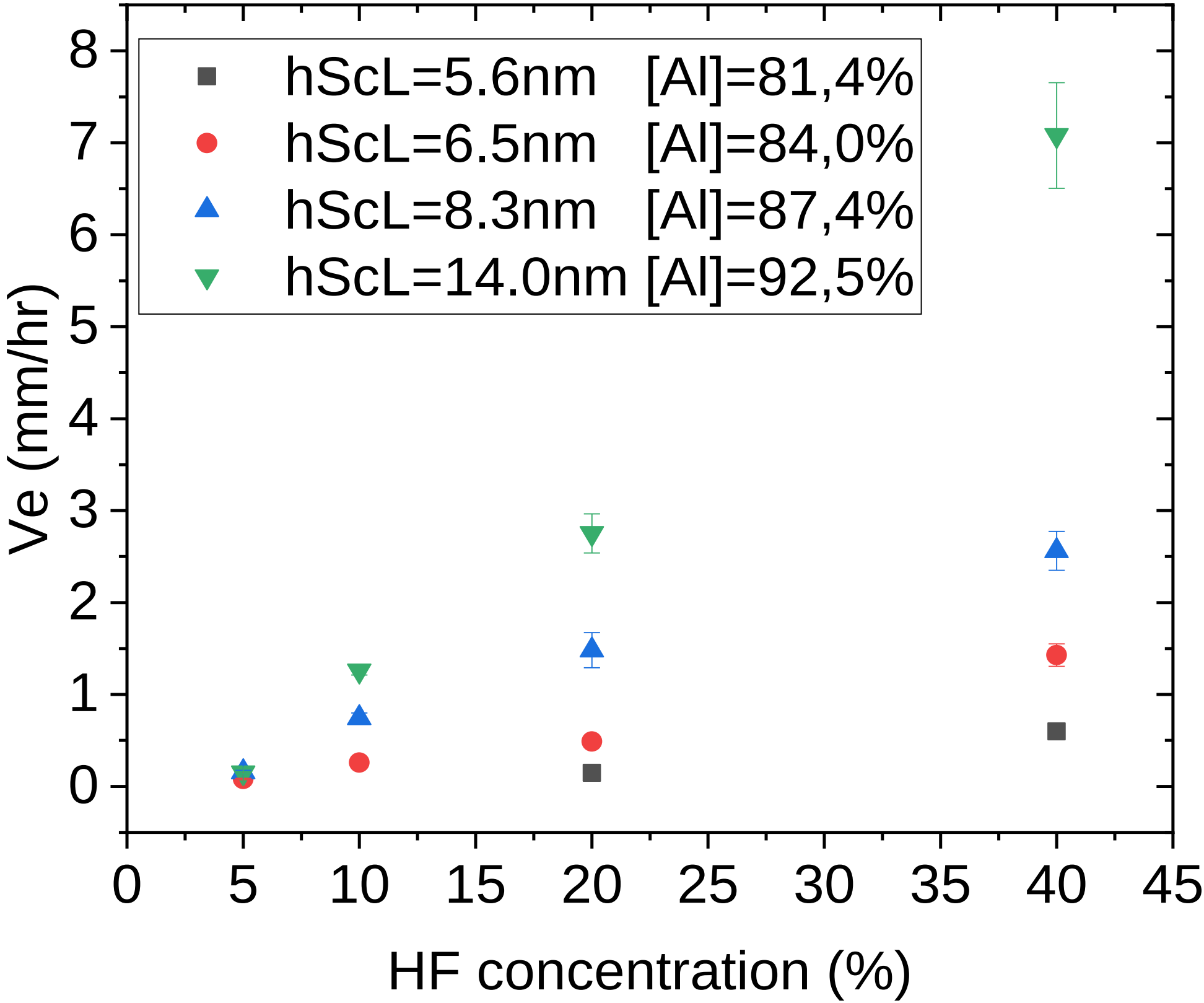
hScL=5.6nm [Al]=81,4%
hScL=6.5nm [Al]=84,0%
hScL=8.3nm [Al]=87,4%
hScL=14.0nm [Al]=92,5%
Ve (mm/hr)
HF concentration (%)
0
1
2
3
4
5
6
7
8
0
5
10
15
20
25
30
35
40
45

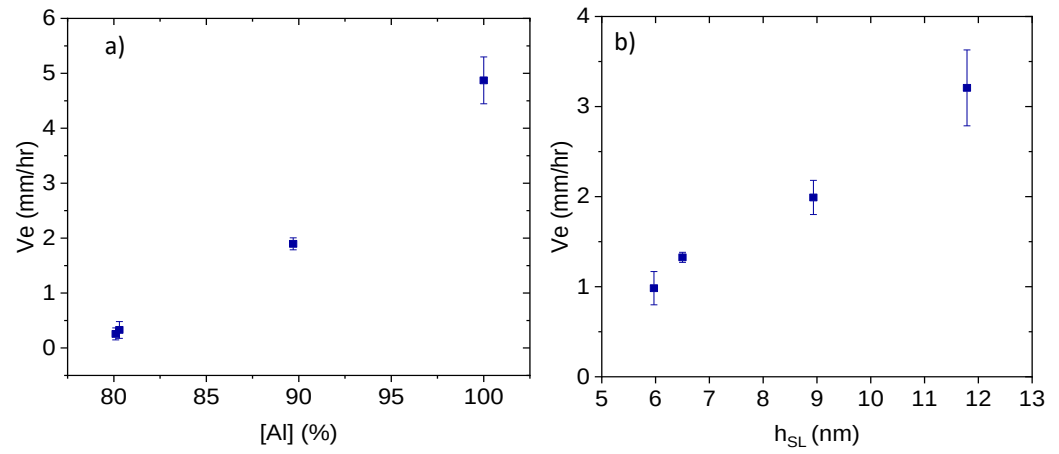
a)
Ve (mm/hr)
[Al] (%)
b)
Ve (mm/hr)
$h_{SL}$ (nm)

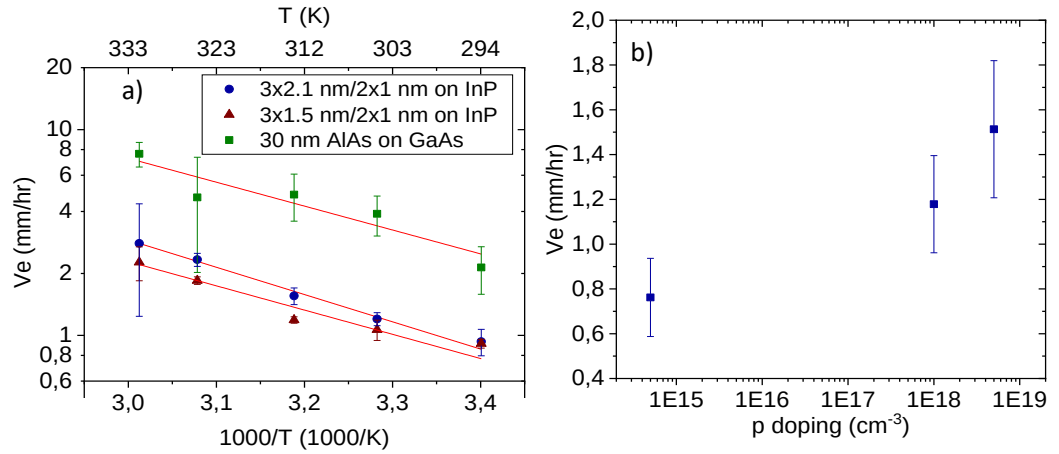
T (K)
333
323
312
303
294
a)
3x2.1 nm/2x1 nm on InP
3x1.5 nm/2x1 nm on InP
30 nm AlAs on GaAs
Ve (mm/hr)
20
10
8
6
4
2
1
0,8
0,6
3,0
3,1
3,2
3,3
3,4
1000/T (1000/K)
b)
Ve (mm/hr)
2,0
1,8
1,6
1,4
1,2
1,0
0,8
0,6
0,4
1E15
1E16
1E17
1E18
1E19
p doping (cm-3)

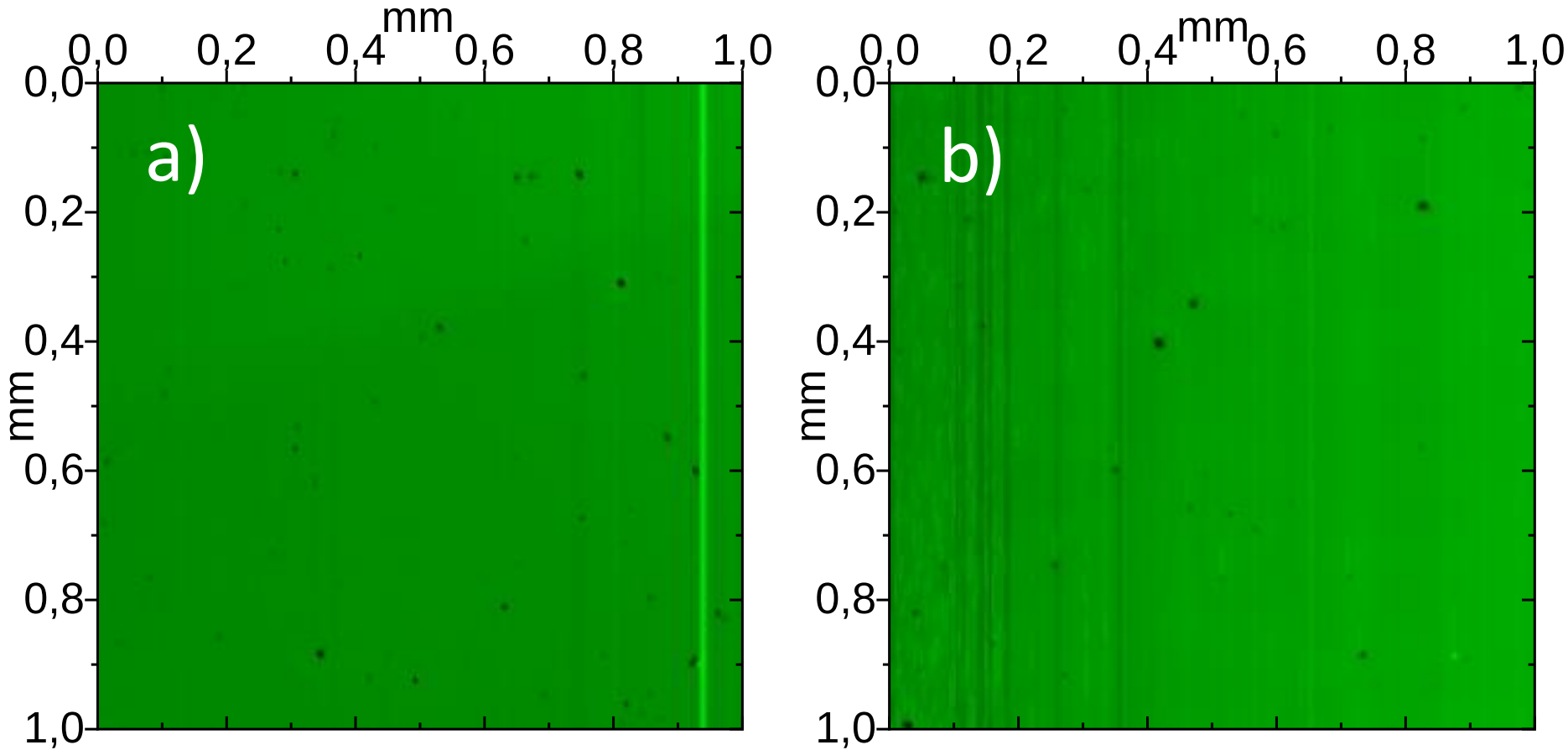
mm
0,0
0,2
0,4
0,6
0,8
1,0
a)
b)

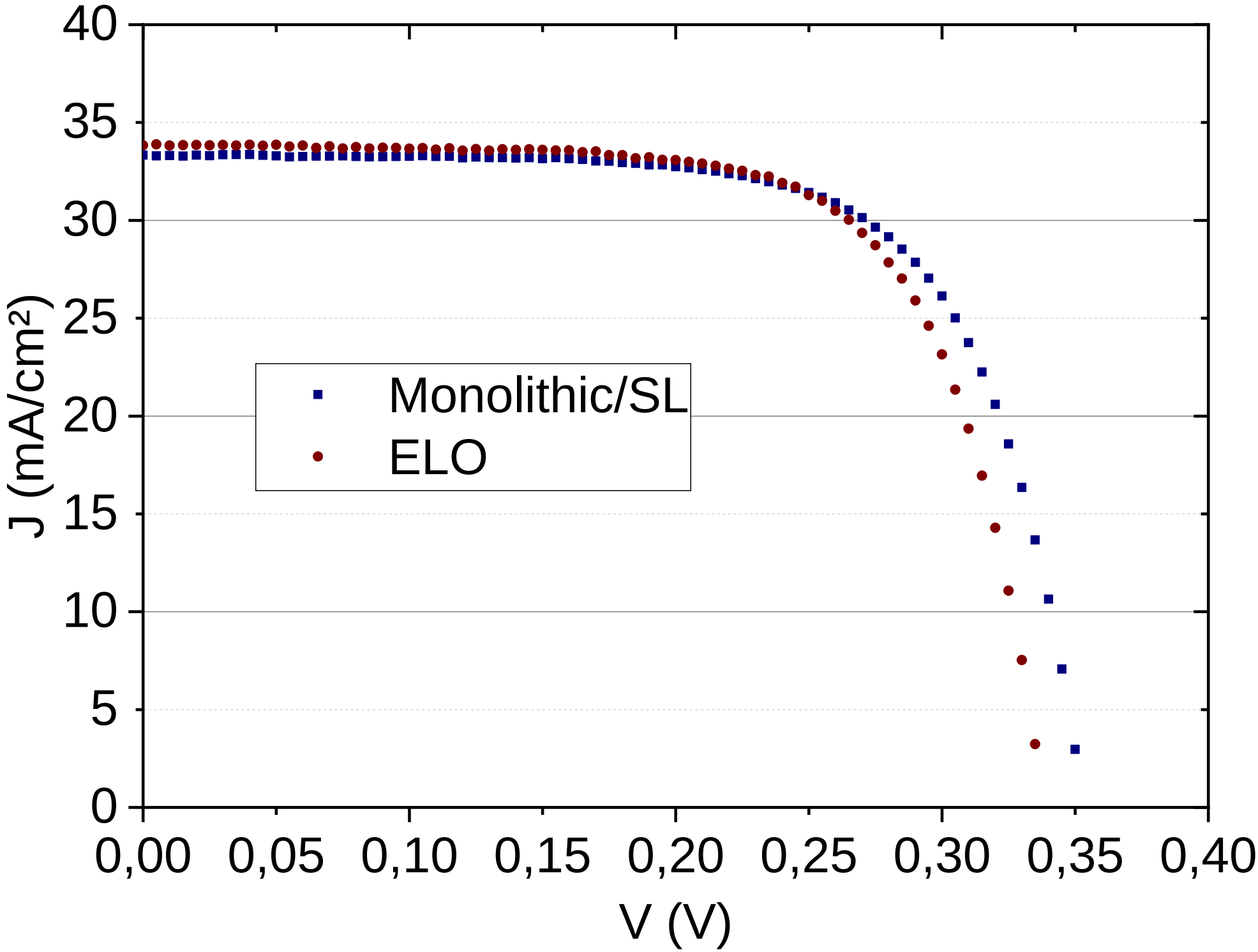
40
35
30
25
20
15
10
5
0
J (mA/cm²)
Monolithic/SL
ELO
0,00
0,05
0,10
0,15
0,20
0,25
0,30
0,35
0,40
V (V)